Available online at www.sciencedirect.com
SCIENCE DIRECT®
Journal of Geodynamics 39 (2005) 512–526
JOURNAL OF GEODYNAMICS
http://www.elsevier.com/locate/jog

On the estimation of a multi-resolution representation of the gravity field based on spherical harmonics and wavelets

M. Schmidt [a,*], O. Fabert [a], C.K. Shum [b]

[a] *Deutsches Geodätisches Forschungsinstitut, Marstallplatz 8, D-80539 München, Germany*
[b] *Laboratory for Space Geodesy and Remote Sensing Research, The Ohio State University, 470 Hitchcock Hall, 2070 Neil Avenue, Columbus, OH 43210, USA*

Accepted 18 April 2005

Abstract

The gravitational potential of the Earth is usually modeled by means of a series expansion in terms of spherical harmonics. However, the computation of the series coefficients requires preferably homogeneous distributed global data sets. Since one of the most important features of wavelet functions is the ability to localize both in the spatial and in the frequency domain, regional and local structures may be modeled by means of a spherical wavelet expansion. In general, applying wavelet theory a given input data set is decomposed into a certain number of frequency-dependent detail signals, which can be interpreted as the building blocks of a multi-resolution representation. On the other hand, there is no doubt that the low-frequency part of the geopotential can be modeled appropriately by means of spherical harmonics. Hence, the main idea of this paper is to derive a combined model consisting of an expansion in spherical harmonics for the low-frequency part and an expansion in spherical wavelets for the remaining medium and high-frequency parts of the gravity field. Furthermore, an appropriate parameter estimation procedure is outlined to solve for the unknown model coefficients.

Keywords: Spherical harmonics; Spherical wavelets; Multi-resolution representation; Bayesian inference

1. Introduction

The determination and the representation of the Earth's gravity field are two of the most important issues of physical geodesy. The knowledge of the Earth's gravity field gives insight into the irregular

* Corresponding author.

0264-3707/$ – see front matter © 2005 Elsevier Ltd. All rights reserved.
doi:10.1016/j.jog.2005.04.007

distribution of masses on and inside the Earth. Furthermore, the geopotential affects satellite orbits and is of great importance for the surveying of the Earth.

Regional gravity field modeling is very useful for the determination of precise geoid undulations, as needed for the reduction of measured GPS heights (Torge, 2001, p. 281). Global and regional representations of the geopotential can also be used for comparisons with geodynamic data sets, e.g. hydrological models.

It is well known that spherical harmonics are an appropriate tool for modeling the low-frequency part of the gravity field. Furthermore, the modern gravity satellite missions like CHAMP or GRACE allow a precise determination of the corresponding series (Stokes) coefficients. However, in order to calculate a high-resolution gravity model, the satellite data has to be combined with terrestrial and/or airborne gravity measurements; see, e.g. Kern (2003). Whereas satellite data is almost globally distributed, unfortunately terrestrial and airborne observations are always restricted to certain regions or local areas. Nevertheless, the computation of the Stokes coefficients requires preferably homogeneous distributed global data sets. Hence, we are interested in an alternative to the classical series expansion in spherical harmonics, namely a representation, which consists of a global trend, more or less computed from the satellite data, and additional signal parts containing the regional and local information derived from terrestrial and airborne data sets. Such a model means a *multi-resolution representation* of the gravity field. In the last years several approaches were pursued to generate multi-resolution representations of the geopotential. Kusche (2002) presents an overview of geodetic concepts concerning the determination and representation of the gravity field. Our approach, described in the following, is based on the spherical wavelet theory derived by the Geomathematics Group of the University of Kaiserslautern, Germany; see Freeden (1999), Freeden et al. (1998) and the references therein.

In the spherical wavelet context there are generally two appropriate methods to model the geopotential, namely (1) the *wavelet-only approach*, i.e. the entire frequency spectrum of the gravity field is covered by a series expansion in terms of wavelets and (2) the so-called *combined approach*, i.e. the representation is split into an expansion in terms of spherical harmonics for the long-wavelength part and an expansion in terms of wavelets for the medium and the high-frequency parts. One important advantage of the combined approach is the fact that we keep the physical meaning of the low-frequency Stokes coefficients. Recall that, for instance, the coefficients of the second degree are related to the elements of the tensor of inertia; see, e.g. Torge (2001, p. 74).

The following section deals with an introduction into the multi-resolution representation using spherical wavelets. Especially, the approximation error is treated in more detail in order to appraise the quality of different wavelet functions. In Section 3, we discuss the estimation of the unknown parameters of the combined approach, developed in Section 2.2, using Bayesian inference. In order to demonstrate the derived procedure Section 4 presents an example based on EGM 96 gravity anomalies. Finally, in Section 5 we point out some ideas concerning the combination of satellite and terrestrial data.

2. Multi-resolution representation

2.1. Wavelet-only approach

In order to deal with spherical signals and functions, we introduce a three-dimensional cartesian coordinate system K with the origin O at the center of a sphere $\Omega_R \subset \mathrm{IR}^3$ with radius $R > 0$. Moreover,

the two basis vectors $\mathbf{e}_1 = [1,0,0]'$ and $\mathbf{e}_2 = [0,1,0]'$ of K span the equator plane, the third basis vector $\mathbf{e}_3 = [0,0,1]'$ defines the direction to the "north" pole. In this coordinate system the position vector $\mathbf{t} \in \mathrm{IR}^3$ of any observation point $P = P(\mathbf{t})$ may be expressed by means of the *spherical coordinates* λ = longitude, β = latitude and r = radial distance, namely

$$\mathbf{t} = r[\cos\beta\cos\lambda, \cos\beta\sin\lambda, \sin\beta]' = r\mathbf{r}; \tag{1}$$

$\mathbf{r}$ denotes the corresponding unit vector. Next, we introduce a real-valued deterministic function $x(\mathbf{t})$, which is assumed to be harmonic in the exterior of the Earth, i.e. it fulfils the Laplacian differential equation. The solution of *Dirichlet's sproblem* for the outer space Ω_R^{ext} of the sphere Ω_R can be expressed by the series expansion

$$x(\mathbf{t}) = \sum_{n=0}^{\infty} \sum_{m=-n}^{n} X_{n,m}^R Y_{n,m}^R(\mathbf{t}) \tag{2}$$

in terms of the *solid spherical harmonics*

$$Y_{n,m}^R(\mathbf{t}) = \frac{1}{\sqrt{4\pi R}} \left(\frac{R}{r}\right)^{n+1} \left\{ \begin{array}{ll} P_{n,m}(\sin\beta)\cos m\lambda, & \text{for } m = 0, \ldots, n \\ P_{n,|m|}(\sin\beta)\sin|m|\lambda, & \text{for } m = -n, \ldots, -1 \end{array} \right\}; \tag{3}$$

$P_{n,m}(\sin\beta)$ are the associated Legendre functions of degree n and order m. Note, that in Eq. (2) $\mathbf{t} \in \overline{\Omega_R^{\mathrm{ext}}}$ holds, where $\overline{\Omega_R^{\mathrm{ext}}} = \Omega_R^{\mathrm{ext}} \cup \Omega_R$ means the union of the outer space Ω_R^{ext} and the sphere Ω_R. Whereas the Stokes coefficients $X_{n,m}^R$ are characterized by an optimal localization in the frequency (degree) domain, according to the uncertainty relation they do not have any localization property in the spatial domain.

Besides the *spherical harmonics approach* (2) the harmonic function $x(\mathbf{t})$ with $\mathbf{t} \in \overline{\Omega_R^{\mathrm{ext}}}$ can be modeled by means of the *spherical wavelet approach*

$$x(\mathbf{t}) = (\theta_j^R \star x)(\mathbf{t}) + s_j(\mathbf{t}) = x_j(t) + s_j(\mathbf{t}). \tag{4}$$

To be more specific,

$$x_j(\mathbf{t}) = (\theta_j^R \star x)(\mathbf{t}) \tag{5}$$

means the modeled part of $x(\mathbf{t})$ and

$$s_j(\mathbf{t}) = x(\mathbf{t}) - x_j(\mathbf{t}) \tag{6}$$

the *approximation error*; the symbol '$\star$' stands for the spherical convolution. The *modified spherical scaling function*

$$\theta_j^R(\mathbf{t}, \mathbf{t}_p) = \sum_{n=0}^{\infty} \frac{2n+1}{4\pi R^2} \left(\frac{R^2}{r r_p}\right)^{n+1} (\Phi_j(n))^2 P_n(\mathbf{r}'\mathbf{r}_p) \tag{7}$$

of resolution level (scale value, scale index) $j \in \mathrm{IN}_0$ depends on the choice of the Legendre coefficients $\Phi_j(n)$; examples are presented below. The variable $\mathbf{r}'\mathbf{r}_p = \cos\alpha = t$ with $-1 \le t \le 1$ of the Legendre polynomials $P_n(t) = P_{n,0}(t)$ of degree n is equal to the cosine of the spherical distance α between two points $P(\mathbf{r}) = P(\lambda, \beta)$ and $P(\mathbf{r}_p) = P(\lambda_p, \beta_p)$ on the unit sphere Ω. The reason, why Eq. (4) is called the spherical wavelet approach, will become clear in the context of Eq. (23). Note, that operators like the Stokes operator can be easily implemented into Eq. (7); see, e.g. Schmidt et al. (2002).

In the case of the non-band-limited *Abel-Poisson scaling function*, for example, the Legendre coefficients $\Phi_j(n)$ are given as

$$\Phi_j(n) = \exp(-n\sigma 2^{-j}), \tag{8}$$

wherein σ is a finite positive constant. The band-limited *Shannon scaling function* is defined by the Legendre coefficients

$$\Phi_j(n) = \begin{cases} 1 & \text{for} \quad n = 0, \ldots, 2^j - 1 \\ 0 & \text{for} \quad n = 2^j, \ldots, \infty \end{cases} \tag{9}$$

(Freeden, 1999, p. 163). Although spherical scaling functions are global functions and not compactly supported in the spatial domain they are characterized by their property to localize on the sphere. The Shannon scaling function, however, shows undesired global oscillations, which may be reduced by replacing Eq. (9) with the Legendre coefficients

$$\Phi_j(n) = \left\{ \begin{array}{ll} 1 & \text{for} \quad n = 0, \ldots, 2^{j-1} - 1 \\ 2 - 2^{1-j} n & \text{for} \quad n = 2^{j-1}, \ldots, 2^{j-1} \\ 0 & \text{for} \quad n = 2^j, \ldots, \infty \end{array} \right\}; \tag{10}$$

of the so-called *smoothed Shannon scaling function*. A more general version of the smoothed Shannon scaling function includes, like in the Abel-Poisson case (8), a shape parameter σ. In Eq. (10), this parameter is set to $\sigma = 0.5$; see Freeden (1999, p. 165).

The function $x_j(\mathbf{t})$, defined in Eq. (5), reads in the frequency domain

$$x_j(\mathbf{t}) = \sum_{n=0}^{\infty} \sum_{m=-n}^{n} (\Phi_j(n))^2 X^R_{n,m} Y^R_{n,m}(\mathbf{t}); \tag{11}$$

see, e.g. Schmidt (2001, p. 274). Inserting the Eqs. (2) and (11) into Eq. (6) yields

$$s_j(\mathbf{t}) = \sum_{n=0}^{\infty} \sum_{m=-n}^{n} S_j(n) X^R_{n,m} Y^R_{n,m}(\mathbf{t}) \tag{12}$$

with

$$S_j(n) := 1 - (\Phi_j(n))^2. \tag{13}$$

Since the Legendre coefficients $\Phi_j(n)$ are subject to the condition $\lim_{j\to\infty}(\Phi_j(n))^2 = 1$ for all $n \in \mathrm{IN}_0$ (see, e.g. Freeden (1999, p. 155), the approximation error function $s_j(\mathbf{t})$ vanishes for $j \to \infty$. On the other hand, if we assume that the function $x(\mathbf{t})$ is band-limited, such that the upper limit of the first sum in the spherical harmonics expansion (2) is given by a finite value n'', an exact representation of the function can be obtained for

$$(\Phi_j(n))^2 = 1 \quad \text{for} \quad n = 0, \ldots, n''. \tag{14}$$

In fact, according to (9) this condition holds for the Shannon scaling function for any scale index $j > \log_2 n''$. For the Abel-Poisson representation, however, the condition (14) can be fulfilled only for

$j \to \infty$. Substituting (8) for $\Phi_j(n)$ into Eq. (13) yields

$$S_j(n) = 1 - \exp(-n\sigma 2^{1-j}). \tag{15}$$

The squared values of these coefficients are visualized in Fig. 1 for $j = 9$ and different constants σ. The smaller the value for σ is chosen the more decreases the approximation error.

The root mean square (rms) value of the approximation error $s_j(\mathbf{t})$ on the sphere Ω_R, i.e. $\mathbf{t} \in \Omega_R$, is defined as

$$\mathrm{rms}(s_j) := \left(\frac{1}{4\pi R^2} \int_{\Omega_R} |s_j(\mathbf{t})|^2 \, \mathrm{d}\omega_R(\mathbf{t}) \right)^{1/2}, \tag{16}$$

where $\mathrm{d}\omega_R(\mathbf{t}) = R^2 \cos\beta \, \mathrm{d}\beta \, \mathrm{d}\lambda$ denotes the surface element on Ω_R. By substituting Eqs. (12) and (13) for $s_j(\mathbf{t})$ into Eq. (16) we obtain under the consideration of the orthogonality condition for the solid spherical harmonics (3) with $r = R$ the result

$$\mathrm{rms}(s_j) = \left(\frac{1}{4\pi} \sum_{n=0}^{\infty} (S_j(n))^2 C_x(n) \right)^{1/2}, \tag{17}$$

wherein

$$C_x(n) = \frac{1}{R^2} \sum_{m=-n}^{n} |X_{n,m}^R|^2 \tag{18}$$

are the *degree variances* of the function $x(\mathbf{t})$; see, e.g. Heiskanen and Moritz (1967, p. 259). Fig. 2 shows the product $(S_j(n))^2 C_x(n)$ in dependence on the degree n for different scale values j. The coarser the resolution, i.e. the smaller the scale value, the worse the approximation and the larger the root mean square value $\mathrm{rms}(s_j)$. Hence, even if we assume that the function $x(\mathbf{t})$ is band-limited, we end up with an approximation error. If we choose, for example, the Abel-Poisson scaling function with $j = 9$ and $\sigma = 0.08$ to approximate the geoid undulations $x(\mathbf{t}) = N(\mathbf{t})$ of EGM 96 according to Eq. (4) we obtain $\mathrm{rms}(s_9) = 3.4$ cm. As can be seen from Fig. 2, especially in the low-frequency range the values for $(S_j(n))^2 C_x(n)$ are considerable.

In the next step, we introduce the erroneous *observed signal* $y(\mathbf{t})$ which replaces the deterministic function $x(\mathbf{t})$ on the left hand side of Eq. (4). In order to keep this equation consistent an additional error

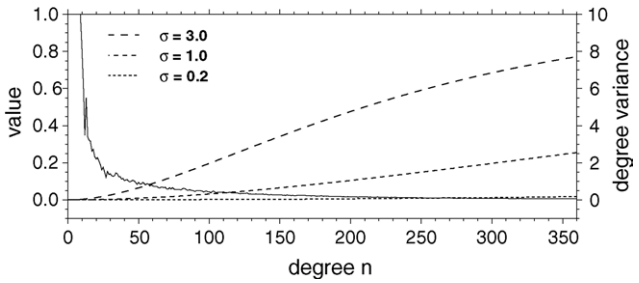

Fig. 1. Coefficients $(S_9(n))^2$ in the Abel-Poisson case with three different σ values. The solid line means the function $C_x(n)$ of degree variances for the geoid undulations of EGM 96.

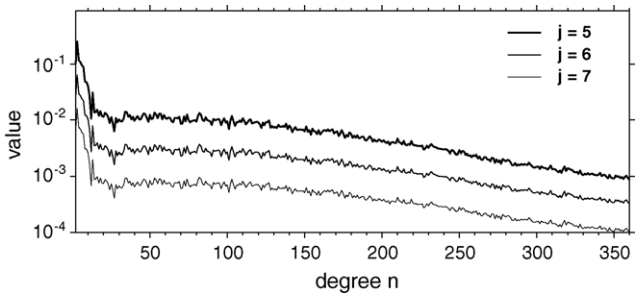

Fig. 2. Values of the product $(S_j(n))^2 C_x(n)$ in the Abel-Poisson case for three different scale indices j and $\sigma = 0.08$.

function $e(\mathbf{t})$ has to be considered. Hence, the general observation equation reads

$$y(\mathbf{t}) + e(\mathbf{t}) = x_j(\mathbf{t}) + s_j(\mathbf{t}), \tag{19}$$

wherein the unknown function $x_j(\mathbf{t})$ again can be modeled by the convolution (5). Note, that Eq. (19) includes two different kinds of errors, namely the stochastic measurement error $e(\mathbf{t})$ and the non-stochastic approximation error $s_j(\mathbf{t})$.

The basic idea of the *multi-resolution representation* is to split a given input signal into a smoothed version and a certain number of band-pass signals by *successive low-pass filtering*. In order to explain this procedure in more detail, we set $j =: I + 1$ in Eq. (19), i.e.

$$y(\mathbf{t}) + e(\mathbf{t}) = x_{I+1}(\mathbf{t}) + s_{I+1}(\mathbf{t}), \tag{20}$$

and introduce the decomposition

$$x_{I+1}(\mathbf{t}) = x_I(\mathbf{t}) + g_I(\mathbf{t}), \tag{21}$$

wherein $x_I(\mathbf{t})$ is a smoothed version of the function $x_{I+1}(\mathbf{t})$. Consequently, the *detail signal* $g_I(\mathbf{t})$ of resolution level I contains the removed high-frequency parts of $x_{I+1}(\mathbf{t})$. In the next step, the function $x_I(\mathbf{t})$ is decomposed into the smoothed version $x_{I-1}(\mathbf{t})$ and the detail signal $g_{I-1}(\mathbf{t})$ of level $I-1$ according to $x_I(\mathbf{t}) = x_{I-1}(\mathbf{t}) + g_{I-1}(\mathbf{t})$. If we proceed in the same manner until resolution level i', we end up with the decomposition

$$x_{I+1}(\mathbf{t}) = x_{i'}(\mathbf{t}) + \sum_{i=i'}^{I} g_i(\mathbf{t}), \tag{22}$$

which is called the multi-resolution representation of the function $x_{I+1}(\mathbf{t})$. The substitution of this result into the observation Eq. (20), i.e.

$$y(\mathbf{t}) + e(\mathbf{t}) = x_{i'}(\mathbf{t}) + \sum_{i=i'}^{I} g_i(\mathbf{t}) + s_{I+1}(\mathbf{t}), \tag{23}$$

yields the multi-resolution representation of the observed signal $y(\mathbf{t})$. To be more specific, the detail signals $g_i(\mathbf{t})$ with $i = i', \ldots, I$ are computed by means of the spherical convolutions

$$g_i(\mathbf{t}) = (\psi_i^R \star \psi_i^R \star x)(\mathbf{t}). \tag{24}$$

The Legendre coefficients $\Psi_i(n)$ of the *spherical wavelet function*

$$\psi_i^R(\mathbf{t},\mathbf{t}_p)=\sum_{n=0}^{\infty}\frac{2n+1}{4\pi R^2}\left(\frac{R^2}{rr_p}\right)^{n+1}\Psi_i(n)P_n(\mathbf{r}'\mathbf{r}_p) \tag{25}$$

are defined by the *two-scale relation*

$$\Psi_i(n)=\sqrt{(\Phi_{i+1}(n))^2-(\Phi_i(n))^2}; \tag{26}$$

see, e.g. Freeden (1999, p. 177). As an example for a spherical wavelet function the *smoothed Shannon wavelet* is illustrated in Fig. 3 for different scale values i. These functions are computed according to Eqs. (25) and (26) by use of Eq. (10) for $j=:i$ and $j=:i+1$. In the frequency domain the smoothed

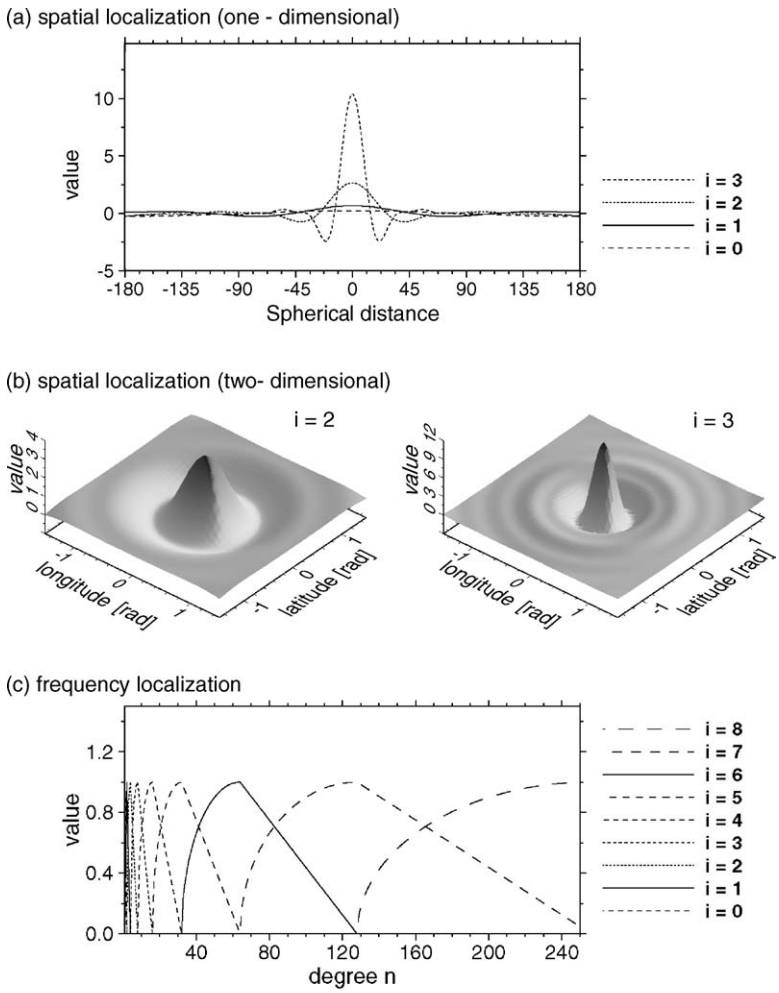

Fig. 3. Smoothed Shannon wavelet with shape parameter $\sigma=0.5$ for different scale indices i; see Freeden (1999, p. 191).

Shannon wavelets are compactly supported or strictly band-limited, respectively, i.e. only a few Legendre coefficients are not equal to zero (Fig. 3c). Since every wavelet function $\psi_i^R(\cdot,\cdot)$ is related to a certain frequency-band, the corresponding detail signal $g_i(\mathbf{t})$ is a band-pass filtered version of the input signal. Hence, Eq. (23) states, that the sum of the observed signal $y(\mathbf{t})$ and the measurement error $e(\mathbf{t})$ is split into a low-pass signal $x_{i'}(\mathbf{t})$, a number of band-pass signals $g_i(\mathbf{t})$ with $i = i', \ldots, I$ and the non-stochastic approximation error $s_{I+1}(\mathbf{t})$.

2.2. Combined approach

In the previous subsection, according to the Eqs. (5) and (7), the function $x_{I+1}(\mathbf{t})$ was modeled as a spherical convolution

$$x_{I+1}(\mathbf{t}) = (\theta_{I+1}^R \star x)(\mathbf{t})$$

of the function $x(\mathbf{t}_p)$, for instance the disturbing potential of the Earth, with the modified spherical scaling function

$$\theta_{I+1}^R(\mathbf{t},\mathbf{t}_p) = \sum_{n=0}^{\infty} \frac{2n+1}{4\pi R^2}\left(\frac{R^2}{rr_p}\right)^{n+1} (\Phi_{I+1})(n))^2 P_n(\mathbf{r}'\mathbf{r}_p).$$

On the other hand, it is well known that spherical harmonics are an appropriate tool to model the low-frequency part of the geopotential. Hence, we now deal with a *combined approach* consisting of an expansion in terms of spherical harmonics until degree and order n' and a spherical wavelet representation for the remaining medium and high-frequency parts of the gravity field. The observation equation of the *combined approach* reads

$$y(\mathbf{t}) + e(\mathbf{t}) = \sum_{n=0}^{n'} \sum_{m=-n}^{n} X_{n,m}^R Y_{n,m}^R(\mathbf{t}) + (\theta_{I+1}^R \star x)(\mathbf{t}) + s_{I+1}(\mathbf{t}), \tag{27}$$

wherein the modified scaling function $\theta_{I+1}^R(\cdot,\cdot)$ is now defined as

$$\theta_{I+1}^R(\mathbf{t},\mathbf{t}_p) = \sum_{n=n'+1}^{\infty} \frac{2n+1}{4\pi R^2}\left(\frac{R^2}{rr_p}\right)^{n+1} (\Phi_{I+1}(n))^2 P_n(\mathbf{r}'\mathbf{r}_p); \tag{28}$$

see, e.g. Kusche (2002, p. 32). Note, that in Eq. (27) the approximation error $s_{I+1}(\mathbf{t})$ generally differs from the corresponding approximation error of the wavelet-only approach (23).

For the numerical evaluation of the last two terms on the right hand side of Eq. (27) we assume now that the function $x(\mathbf{t})$ is band-limited, i.e. the spherical harmonics representation (2) of $x(\mathbf{t})$ would provide $X_{n,m}^R = 0$ for $n > n''$ and $n'' > n'$. Furthermore, we substitute the Legendre coefficients (10) of the smoothed Shannon scaling function for $\Phi_{I+1}(n)$ into Eq. (28). Under these assumptions the highest detail level I is restricted to

$$I \geq \log_2(n'' + 1). \tag{29}$$

Hence, due to Eq. (14) the approximation error function $s_{I+1}(\mathbf{t})$ in Eq. (27) vanishes. Next, an appropriate *admissible system* of discrete computation points $P(\mathbf{t}_{I,k})$ with $k = 1, \ldots, N_I$ and $\mathbf{t}_{I,k} \in \Omega_R$ is chosen, so that the band-limited function $x(\mathbf{t})$ can be modeled exactly by a finite series expansion; see, e.g. Driscoll and

Healy (1994). Thus, the observation Eq. (27) reduces to

$$y(\mathbf{t}) + e(\mathbf{t}) = \sum_{n=0}^{n'} \sum_{m=-n}^{n} X_{n,m}^{R} Y_{n,m}^{R}(t) + \sum_{k=1}^{N_I} d_{I,k} \theta_{I+1}^{R}(\mathbf{t}, \mathbf{t}_{I,k}) \tag{30}$$

with $\theta_{I+1}^{R}(\mathbf{t}, \mathbf{t}_{I,k})$ defined in Eq. (28) and $\mathbf{t} \in \overline{\Omega_R^{\text{ext}}}$. The Stokes coefficients $X_{n,m}^{R}$, which do not have any spatial information, are the parameters of the global trend mentioned in the introduction. In contrast the coefficients $d_{I,k}$ reflect the regional or local behavior of the input signal because they are directly related to the points $P(\mathbf{t}_{I,k})$ with $\mathbf{t}_{I,k} \in \Omega_R$. Solving Eq. (30) for the unknown coefficients $d_{I,k}$ with $k = 1, \ldots, N_1$ means the *initial step* of the so-called pyramid algorithm; see, e.g. Schmidt et al. (2005). In the first *pyramid step* the altogether N_{I-1} coefficients $d_{I-1,k'}$ of level $I-1$, related to the computation points $P(\mathbf{t}_{I-1,k'})$ with $k' = 1$, $\ldots$, N_{I-1} and $\mathbf{t}_{I-1,k'} \in \Omega_R$, are calculated from the N_I coefficients $d_{I,k}$. Due to $N_{I-1} < N_I$ this procedure is based on a down sampling strategy. In general, in the $(I-i)$th pyramid step the N_i coefficients $d_{i,k}$ with $i \in \{i', \ldots, I-1\}$ and $k = 1, \ldots, N_i$, related to the N_i computation points $P(\mathbf{t}_{i,k})$ of the level-i admissible system, are calculated from the N_{i+1} coefficients $d_{i+1,k'}$, related to the N_{i+1} computation points $P(\mathbf{t}_{i+1,k'})$ with $k' = 1, \ldots, N_{i+1}$ of the level-$(i+1)$ admissible system. This procedure reads in matrix formalism

$$\mathbf{d}_i = \mathbf{H}_i \mathbf{d}_{i+1}, \tag{31}$$

wherein $\mathbf{d}_{i+1} = (d_{i+1,k'})$ and $\mathbf{d}_i = (d_{i,k})$ are $N_{i+1} \times 1$ and $N_i \times 1$ vectors of coefficients, respectively. Furthermore, $\mathbf{H}_i$ means an $N_i \times N_{i+1}$ matrix which acts as a low-pass filter. Frequently *hierarchical* point systems are preferred, so that the set of points $P(\mathbf{t}_{i,k})$ with $k = 1, \ldots, N_i$ is a subset of the set of points $P(\mathbf{t}_{i+1,k'})$ with $k' = 1, \ldots, N_{i+1}$. For more details concerning this decomposition process see, e.g. Schreiner (1997) or Schmidt et al. (2005). But, we finally want to mention again that the Stokes coefficients $X_{n,m}^{R}$ are *global parameters*, whereas the coefficients $d_{i,k}$ of the levels $i = i', \ldots, I$ *are point parameters*.

According to Eq. (24) the band-limited detail signals $g_i(\mathbf{t})$ with $i = i', \ldots, I$ are computed from

$$g_i(\mathbf{t}) = \sum_{k=1}^{N_i} d_{i,k} (\psi_i^R \star \psi_i^R)(\mathbf{t}, \mathbf{t}_{i,k}). \tag{32}$$

Analog to Eq. (23) the observation Eq. (30) can be rewritten as a multi-resolution representation, namely

$$y(\mathbf{t}) + e(\mathbf{t}) = x_{0,\ldots,n'}(\mathbf{t}) + \sum_{i=i'}^{I} g_i(\mathbf{t}), \tag{33}$$

where

$$x_{0,\ldots,n'}(\mathbf{t}) := \sum_{n=0}^{n'} \sum_{m=-n}^{n} X_{n,m}^{R} Y_{n,m}^{R}(\mathbf{t}) \tag{34}$$

denotes the spherical harmonics part. Due to the Eqs. (10) and (26) the value i' is chosen such that

$$i' \leq \log_2(n' + 1) \tag{35}$$

holds. Note, that due to Eq. (31) the coefficients of the detail signals of different resolution levels are depending on each other. Hence, to apply parameter estimation techniques we use the observation Eq.

(30). In order to solve Eq. (30) for the unknowns and to apply the pyramid algorithm using the formulae (31) and (32) the number N_i of points of the level-i admissible system with $i \in \{i', \ldots, I\}$ is generally restricted to

$$N_i \geq 2^{2i+2}. \tag{36}$$

This inequality can be derived from the Eqs. (9) and (10) in the case of band-limited scaling functions. If the equal sign holds in Eq. (36) the admissible point system is called *fundamental system*; see also e.g. Schmidt et al. (2005).

3. Parameter estimation

Geodetic measurements are invariably attached to *scattered* observation points $P(\mathbf{t}_p)$ with $\mathbf{t}_p \in \overline{\Omega_R^{\text{ext}}}$ and $p = 1, \ldots, N$. With the abbreviations $y(\mathbf{t}_p) =: y_p$, $e(\mathbf{t}_p) =: e_p$, $Y_{n,m}^R(\mathbf{t}_p) =: Y_{n,m;p}^R$ and $\theta_{I+1}^R(\mathbf{t}_p, \mathbf{t}_{I,k}) =: \theta_{I+1;p,k}^R$ the observation Eq. (30) reads

$$y_p + e_p = \sum_{n=0}^{n'} \sum_{m=-n}^{n} X_{n,m}^R Y_{n,m;p}^R + \sum_{k=1}^{N_I} d_{I,k} \theta_{I+1;p,k}^R. \tag{37}$$

By introducing the $N \times 1$ observation vector $\mathbf{y} = (y_p)$, the $N \times 1$ vector $\mathbf{e} = (e_p)$ of measurement errors, the $N \times u_1$ coefficient matrix $\mathbf{X}_1 = (Y_{n,m;p}^R)$ and the $N \times u_2$ coefficient matrix $\mathbf{X}_2 = (\theta_{I+1;p,k}^R)$ as well as the $u_1 \times 1$ vector $\boldsymbol{\beta}_1 = (X_{n,m}^R)$ of the $(n'+1)^2 =: u_1$ Stokes coefficients $X_{n,m}^R$ and the $u_2 \times 1$ vector $\boldsymbol{\beta}_2 = (d_{I,k}) = \mathbf{d}_I$ of the $N_I =: u_2$ scaling coefficients $d_{I,k}$, we obtain the linear model

$$\mathbf{y} + \mathbf{e} = \mathbf{X}_1 \boldsymbol{\beta}_1 + \mathbf{X}_2 \boldsymbol{\beta}_2 \quad \text{with} \quad D(\mathbf{y}) = \sigma^2 \boldsymbol{\Sigma}_y \tag{38}$$

of the combined approach; herein σ^2 and $\boldsymbol{\Sigma}_y$ are denoted as the variance of unit weight and the matrix of cofactors, respectively; $\boldsymbol{\Sigma}_y$ is assumed to be positive definite. Since the smoothed Shannon scaling function is according to Eq. (10) band-limited, the rank of the $u \times u$ normal equation matrix

$$\mathbf{N} = \begin{bmatrix} \mathbf{N}_{1,1} & \mathbf{N}_{1,2} \\ \mathbf{N}_{2,1} & \mathbf{N}_{2,2} \end{bmatrix} \tag{39}$$

with $\mathbf{N}_{k,l} = \mathbf{X}_k' \boldsymbol{\Sigma}_y^{-1} \mathbf{X}_l = \mathbf{N}_{l,k}'$, $k, l \in \{1,2\}$ and $u = u_1 + u_2$ is given by rank $\mathbf{N} = 2^{2I+2}$, i.e. a rank deficiency of $r = u - 2^{2I+2}$ exists. Hence (38), means a *linear model not of full rank* (Koch, 1999, p. 181). Note, that we do not deal with regularization problems here. If we consider, that due to the Eq. (28), the spherical wavelet model part $\mathbf{X}_2 \boldsymbol{\beta}_2$ is independent of the spherical harmonics part $\mathbf{X}_1 \boldsymbol{\beta}_1$, the sub-matrix $\mathbf{N}_{1,2}$ vanishes. Hence, the normal equation system degenerates into two parts and allows a separate determination of the estimators $\hat{\boldsymbol{\beta}}_1$ and $\hat{\boldsymbol{\beta}}_2$ of the unknown parameter vectors $\boldsymbol{\beta}_1$ and $\boldsymbol{\beta}_2$. To overcome the rank deficiency problem mentioned before, the normal equation system might be solved by means of *Bayesian inference*, i.e. we assume that in the linear model (38) the unknown parameter vectors $\boldsymbol{\beta}_k$ with $k \in \{1,2\}$ are random vectors, which might be normally distributed according to

$$\boldsymbol{\beta}_k \sim N(\boldsymbol{\mu}_k, \sigma^2 \boldsymbol{\Sigma}_k). \tag{40}$$

Note, that the parameters $\boldsymbol{\mu}_k$ and $\sigma^2\boldsymbol{\Sigma}_k$ of the normal distribution are equal to the vector $E(\boldsymbol{\beta}_k)$ of the expectation value and the covariance matrix $D(\boldsymbol{\beta}_k)$ of the random vector $\boldsymbol{\beta}_k$, respectively. In order to derive the *Bayes estimator* $\hat{\boldsymbol{\beta}}_k$ of $\boldsymbol{\beta}_k$ we assume that besides the unknown parameter vectors $\boldsymbol{\beta}_k$ the observation vector $\mathbf{y}$ is, as usual, normally distributed, too. Hence, the application of the *Bayes' theorem* leads to the solution

$$\hat{\boldsymbol{\beta}}_k = (\mathbf{N}_{k,k} + \boldsymbol{\Sigma}_k^{-1})^{-1}(\mathbf{X}_k'\boldsymbol{\Sigma}_k^{-1}\mathbf{y} + \boldsymbol{\Sigma}_k^{-1}\boldsymbol{\mu}_k); \tag{41}$$

see, e.g. Koch (2000, p. 125). The corresponding covariance matrix $D(\hat{\boldsymbol{\beta}}_k)$ is given as

$$D(\hat{\boldsymbol{\beta}}_k) = \sigma^2(\mathbf{N}_{k,k} + \boldsymbol{\Sigma}_k^{-1})^{-1}. \tag{42}$$

Note, that besides the estimation (41) of the unknown parameter vectors, the Bayes estimator of the variance σ^2 is also computable; see, e.g. Koch (2000, p. 117).

As mentioned before the calculation of the estimator (41) means the initial step of the pyramid algorithm. The estimator $\hat{\mathbf{d}}_i$ of the vector $\mathbf{d}_i$ of the $(I-i)$th pyramid step with $i \in \{i', \ldots, I-1\}$ is obtained from Eq. (31) considering $\hat{\mathbf{d}}_I = \hat{\boldsymbol{\beta}}_2$, i.e. successive substitution gives

$$\hat{\mathbf{d}}_i = \mathbf{H}_i\mathbf{H}_{i+1}\ldots\mathbf{H}_{I-1}\hat{\mathbf{d}}_I =: \mathbf{A}_i\hat{\boldsymbol{\beta}}_2. \tag{43}$$

Note, that for $i = I$ the coefficient matrix $\mathbf{A}_I$ equals the $N_I \times N_I$ unit matrix $\boldsymbol{I}_{N_I}$, i.e. $\mathbf{A}_I = \mathbf{I}_{N_I}$. In order to estimate the detail signals $g_i(\mathbf{t})$, according to Eq. (32) we define the $N \times N_i$ matrix $\mathbf{Q}_i = ((\psi_i^R \star \psi_i^R)(\mathbf{t}_p, \mathbf{t}_{i,k}))$ and obtain considering the right hand side of Eq. (43)

$$\hat{\mathbf{g}}_i = \mathbf{Q}_i\hat{\mathbf{d}}_i = \mathbf{Q}_i\mathbf{A}_i\hat{\boldsymbol{\beta}}_2 \tag{44}$$

with $i = i', \ldots, I$. Herein $\hat{\mathbf{g}}_i$, means the estimator of the $N \times 1$ vector $\mathbf{g}_i = (g_i(\mathbf{t}_p))$ of the detail signal values $g_i(\mathbf{t}_p)$ in the observation points $P(\mathbf{t}_p)$. Applying the law of error propagation to Eq. (44) gives under the consideration of (42) the covariance matrix

$$D(\hat{\mathbf{g}}_i) = \sigma^2\mathbf{Q}_i\mathbf{A}_i(\mathbf{N}_{k,k} + \boldsymbol{\Sigma}_k^{-1})^{-1}\mathbf{A}_i'\mathbf{Q}_i' \tag{45}$$

of the estimated detail vector $\hat{\mathbf{g}}_i$. In the same manner we obtain the covariance matrix

$$C(\hat{\mathbf{g}}_i, \hat{\mathbf{g}}_j) = \sigma^2\mathbf{Q}_i\mathbf{A}_i(\mathbf{N}_{k,k} + \boldsymbol{\Sigma}_k^{-1})^{-1}\mathbf{A}_j'\mathbf{Q}_j' \tag{46}$$

between the estimated detail vectors $\hat{\mathbf{g}}_i$ and $\hat{\mathbf{g}}_j$ of levels i and j. Finally, according to Eq. (33) the estimated multi-resolution representation of the vector $\mathbf{x} = (x(\mathbf{t}_p))$ reads

$$\hat{\mathbf{x}} = \hat{\mathbf{x}}_{0,\ldots,n'} + \sum_{i=i'}^{I}\hat{\mathbf{g}}_i, \tag{47}$$

wherein $\hat{\mathbf{x}}_{0,\ldots,n'} = (\hat{x}_{0,\ldots,n'}(\mathbf{t}_p))$ means the estimation of the $N \times 1$ vector $\mathbf{x}_{0,\ldots,n'} = (x_{0,\ldots,n'}(\mathbf{t}_p))$ of the spherical harmonic signal values (34) computed in the observation points $P(\mathbf{t}_p)$. The *total* (*experimental, empirical*) *variance* of the difference vector

$$\Delta\hat{\mathbf{x}} := \hat{\mathbf{x}} - \hat{\mathbf{x}}_{0,\ldots,n'} = \sum_{i=i'}^{I}\hat{\mathbf{g}}_i \tag{48}$$

is defined as

$$\mathrm{var}(\Delta\hat{\mathbf{x}}) = \frac{\Delta\hat{\mathbf{x}}'\Delta\hat{\mathbf{x}}}{N}; \tag{49}$$

see, e.g. Wackernagel (1998, p. 18). Substituting the Eqs. (44) and (48) into Eq. (49) yields

$$\mathrm{var}(\Delta\hat{\mathbf{x}}) = \frac{1}{N}\sum_{i=i'}^{I}\sum_{j=i'}^{I}\hat{\mathbf{g}}_i'\hat{\mathbf{g}}_j = \frac{1}{N}\sum_{i=i'}^{I}\sum_{j=i'}^{I}\hat{\mathbf{d}}_i'\mathbf{Q}_i'\mathbf{Q}_j\hat{\mathbf{d}}_j = \sum_{i=i'}^{I}\sum_{j=i'}^{I}\mathrm{cov}(\hat{\mathbf{g}}_i, \hat{\mathbf{g}}_j). \tag{50}$$

The level variances $\mathrm{cov}(\hat{\mathbf{g}}_i, \hat{\mathbf{g}}_i) = \mathrm{var}(\hat{\mathbf{g}}_i)$ and the *level covariances* $\mathrm{cov}(\hat{\mathbf{g}}_i, \hat{\mathbf{g}}_j)$ for $i \neq j$ can be interpreted as the counterpart to the degree variances of the spherical harmonics approach as defined in Eq. (18).

Note, that generally in contrast to the assumptions made in Eq. (44), the elements of all vectors in Eq. (47) are related to points $P(\mathbf{t}_q)$ with $q = 1, \ldots, M$ and $\mathbf{t}_q \in \overline{\Omega_R^{\mathrm{ext}}}$, which do not necessarily coincide with the observation sites $P(\mathbf{t}_p)$.

4. Numerical example

In this section the combined approach is applied to *gravity anomalies of EGM* 96. In order to demonstrate the method we set $I = 5$ and $n' = 7$ in the observation Eq. (37) for the highest resolution level and the maximum degree of the spherical harmonics part, respectively. Hence, according to Fig. 3c we can resolve signal parts until degree $n = 63$, i.e. the corresponding spherical harmonics representation would contain $64^2 = 4096$ Stokes coefficients $X_{n,m}^R$. Consequently, according to Eq. (36) the number N_5 of points of the level-5 admissible system is restricted to $N_5 \geq 4096$. To be more specific, we choose a level-5 *Reuter grid* with altogether $N_5 = 5180$ points $\mathrm{P}(\mathbf{t}_{5,k})$; Fig. 4 shows, e.g. the level-3 Reuter grid with $N_3 = 317$ points. With $u_1 = (n'+1)^2 = 64$ and $u_2 = N_5 = 5180$ the rank deficiency of the normal equation matrix (39) amounts $r = 1148$. Since Reuter grids are equidistributed point systems on the sphere, i.e. the corresponding integration weights are constant, we set $\Sigma_2 = c\mathbf{I}_{N_l}$ in Eq. (40), wherein c is a positive constant. The solution (41) is computed iteratively by updating the vector $\boldsymbol{\mu}_2$, i.e. in the nth iteration step we calculate

$$\hat{\boldsymbol{\beta}}_k^{(n)} = (\mathbf{N}_{k,k} + \boldsymbol{\Sigma}_k^{-1})^{-1}(\mathbf{X}_k'\boldsymbol{\Sigma}_k^{-1}\mathbf{y} + \boldsymbol{\Sigma}_k^{-1}\hat{\boldsymbol{\beta}}_2^{(n-1)}).$$

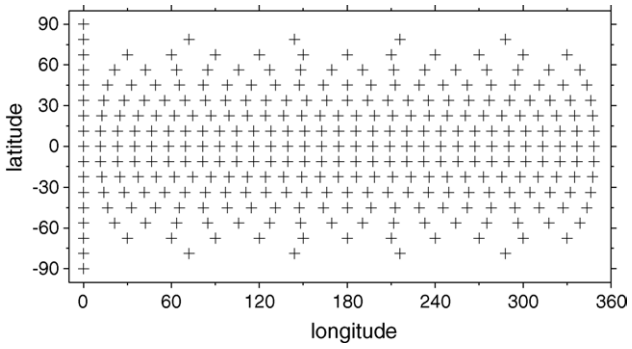

Fig. 4. Level-3 Reuter grid with $N_3 = 317$ points. Reuter grids are non-hierarchical but equidistributed point systems on the sphere; see, e.g. Freeden (1998, p. 171).

In opposite to this procedure a so-called non-informative prior density function is considered for the parameter vector $\boldsymbol{\beta}_1$ of the Stokes coefficients (Koch, 2000, p. 89). If the iteration converges the final estimator $\hat{\boldsymbol{\beta}}_2$ is used to compute the detail vector $\hat{\mathbf{g}}_5$ according to Eq. (44) with $i = 5$ and $\mathbf{A}_5 = \mathbf{I}_{N_5}$. Choosing $i' = 3$ from Eq. (35) the multi-resolution representation (47) reads

$$\hat{\mathbf{x}} = \hat{\mathbf{x}}_{0,\ldots,7} + \hat{\mathbf{g}}_3 + \hat{\mathbf{g}}_4 + \hat{\mathbf{g}}_5. \tag{51}$$

To compute the detail vectors $\hat{\mathbf{g}}_3$ and $\hat{\mathbf{g}}_4$, following Eq. (44), we use level-3 and level-4 Reuter grids with $N_3 = 317$ and $N_4 = 1290$ points, respectively; see Fig. 4. As mentioned in the context of Eq. (30) we want to avoid the approximation error $s_6(\mathbf{t})$, included in Eq. (27). According to Eq. (29) the maximum degree n'' of the input data set is restricted to $n'' = 31$ for $I = 5$. Thus, Fig. 5a shows the gravity anomalies until degree $n'' = 31$. The Fig. 5b and c display the four estimated components $\hat{\mathbf{x}}_{0,\ldots,7}$, $\hat{\mathbf{g}}_3$, $\hat{\mathbf{g}}_4$ and $\hat{\mathbf{g}}_5$ of the multi-resolution representation (51). The deviations (not shown here) between the input signal and the

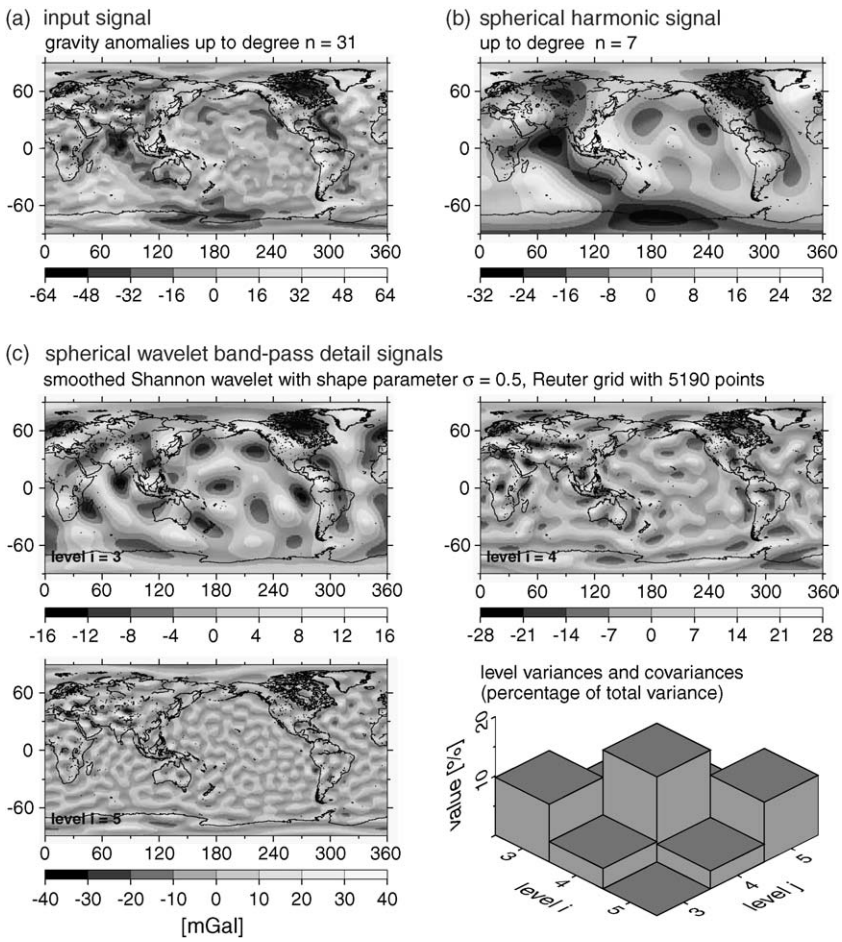

Fig. 5. Input signal, results of the combined estimation according to Eq. (51) as well as level variances and covariances according to Eq. (50).

multi-resolution representation are in the range of the computational accuracy. As can be seen from the bottom panel on the right-hand side of Fig. 5 the values for the level variances $\sigma^2_{\hat{\mathbf{g}}_i}$ with $i = 3$, 4 and 5 are quite similar. Furthermore, according to Fig. 3c the level covariances $\mathrm{cov}(\hat{\mathbf{g}}_i, \hat{\mathbf{g}}_j)$ vanish for $|i - j| > 1$, i.e. $\mathrm{cov}(\hat{\mathbf{g}}_3, \hat{\mathbf{g}}_5) = \mathrm{cov}(\hat{\mathbf{g}}_5, \hat{\mathbf{g}}_3) = 0$.

5. Conclusions and outlook

As mentioned before our underlying objective is to combine satellite data with terrestrial and/or airborne data in order to calculate a high-resolution gravity field. We demonstrated in the previous section that global data sets can be modeled by the multi-resolution representation (47) of the combined approach. Furthermore, Bayesian inference provides appropriate adjustment tools to estimate the unknown model parameters. Due to the gaps in the polar regions the data of the modern satellite gravity missions are almost globally distributed. Schmidt et al. (2005) present the multi-resolution representation of CHAMP disturbing potential data according to Eq. (47) with maximum resolution level $I = 4$ at satellite altitude. However, in order to combine satellite data with terrestrial data it is meaningful to choose a reference sphere Ω_R close to the real surface of the Earth. This procedure can also be applied, e.g. to monthly solutions of GRACE measurements in order to study hydrological phenomena.

Finally, we want to outline the combination of satellite and terrestrial data in somewhat more detail. Let's assume that the observation equation for the *satellite data* is given by Eq. (37) with highest resolution level $I =: I_s$. Furthermore, we want to incorporate *high-resolution terrestrial data*, just available in a region $\Delta\Omega_R \subset \Omega_R$, in our adjustment procedure. The observation equation for this second kind of measurements is also given by Eq. (37), but with $\mathbf{t}_p \in \Delta\Omega_R$ and highest resolution level $I =: I_t$ with $I_t > I_s$. Note, that probably additional operators, like the Stokes operator, have to be considered, if the observations are functionals of the disturbing potential. The two kinds of observation equations, mentioned before, contain besides the Stokes coefficients $X^R_{n,m}$ until degree n' the scaling coefficients $d_{I_s,k}$ and $d_{I_t,k'}$. The relation between these coefficients of two different resolution levels I_s and I_t follows from Eqs. (31) and (43), namely

$$\mathbf{d}_{I_s} = \mathbf{H}_{I_s}\mathbf{H}_{I_s+1}\ldots\mathbf{H}_{I_t-1}\mathbf{d}_{I_t}.$$

Naturally, neglecting edge effects, only these coefficients $d_{I_t,k'}$ are estimable, which are related to points $P(\mathbf{t}_{I_t,k'})$ with $\mathbf{t}_{I_t,k'} \in \Delta\Omega_R$.

An appropriate procedure to solve this problem of combining satellite and terrestrial data in the framework presented before will be treated by the authors in much more detail in a forthcoming publication.

References

Driscoll, J.R., Healy, R.M., 1994. Computing fourier transforms and convolutions on the 2-sphere. Adv. Appl. Math. 15, 202–250.

Freeden, W., 1999. Multiscale Modelling of Spaceborne Geodata. Teubner, Stuttgart.

Freeden, W., Gervens, T., Schreiner, M., 1998. Constructive Approximation on the Sphere (With Applications to Geomathematics). Clarendon Press, Oxford.

Heiskanen, W., Moritz, H., 1967. Physical Geodesy. Freeman, San Francisco.

Kern, M., 2003. An analysis of the combination and downward continuation of satellite, airborne and terrestrial gravity data. Ph.D. Thesis. UCGE Report No. 20172, University of Calgary.

Koch, K.R., 1999. Parameter Estimation and Hypothesis Testing in Linear Models. Springer, Berlin.
Koch, K.R., 2000. Einführung in die Bayes-Statistik. Springer, Berlin.
Kusche, J., 2002. Inverse probleme bei der Gravitationsfeldbestimmung mittels SST- und SGG-Satellitenmissionen. Postdoctoral thesis. German Geodetic Commission, München.
Schmidt, M., 2001. Grundprinzipien der Wavelet-Analyse und Anwendungen in der Geodäsie. Postdoctoral thesis. Shaker, Aachen.
Schmidt, M., Fabert, O., Shum, C.K., 2002. Multi-resolution representation of the gravity field using spherical wavelets. In: Weikko A. Heiskanen Symposium, Ohio State University, Columbus.
Schmidt, M., Fabert, O., Shum, C.K., 2005. Towards the estimation of a multi-resolution representation of the gravity field based on spherical wavelets. In: Sansò, F. (Ed.), A Window on the Future of Geodesy, vol. 128. Springer, pp. 362–367.
Schreiner, M., 1997. Pyramid Scheme for Spherical Wavelets. Berichte der Arbeitsgruppe Technomathematik, No. 170, University of Kaiserslautern.
Torge, W., 2001. Geodesy. de Gruyter, Berlin.
Wackernagel, H., 1998. Multivariate Geostatistics. Springer, Berlin.